International Journal of Neural Systems, Vol. 0, No. 0 (2015) 1–18

A COMPUTATIONAL FRAMEWORK FOR REALISTIC RETINA MODELING

Pablo Martínez-Cañada, Christian Morillas, Begoña Pino, Eduardo Ros and Francisco Pelayo*
Department of Computer Architecture and Technology. CITIC-UGR
University of Granada, Spain
{*pablomc,cmg,bpino,eros,fpelayo*}*@ugr.es*

Computational simulations of the retina have led to valuable insights about the biophysics of its neuronal activity and processing principles. A great number of retina models have been proposed to reproduce the behavioral diversity of the different visual processing pathways. While many of these models share common computational stages, previous efforts have been more focused on fitting specific retina functions rather than generalizing them beyond a particular model. Here we define a set of computational retinal microcircuits that can be used as basic building blocks for the modeling of different retina mechanisms. To validate the hypothesis that similar processing structures may be repeatedly found in different retina functions, we implemented a series of retina models simply by combining these computational retinal microcircuits. Accuracy of the retina models for capturing neural behavior was assessed by fitting published electrophysiological recordings that characterize some of the best-known phenomena observed in the retina: adaptation to the mean light intensity and temporal contrast, and differential motion sensitivity. The retinal microcircuits are part of a new software platform for efficient computational retina modeling from single-cell to large-scale levels. It includes an interface with spiking neural networks that allows simulation of the spiking response of ganglion cells and integration with models of higher visual areas.

Keywords: computational retina modeling; large-scale retina model; single-cell retina model; retina simulator; visual adaptation; contrast adaptation; adaptation to the mean light intensity; object motion sensitive cells; space-variant Gaussian filter; low-pass temporal filter; single-compartment model; static nonlinearity; short-term plasticity; spiking neural networks.

1. Introduction

Although the retina is one of the most extensively studied neural circuits in the visual system, from the first findings by Cajal[1] up to the present day, many aspects of retinal connectivity are still controversial and certain functional mechanisms are not entirely clear [2–5]. Retinal cells connect in different and complex neural structures that provide a wide repertoire of visual functions. Numerous computational models have been proposed to accurately predict the different retina functionalities on the response to artificial and natural visual patterns. However, the aim has been to perfectly describe the retina behavior observed in a specific physiological experiment rather than extrapolating results. On the contrary, neural simulation tools such as NEST[6], NEURON[7], BRIAN[8] or GENESIS[9], exploit common properties of neurons (e.g., their ionic-selective channels) to provide researchers with a general and unified framework for neural modeling that facilitates the study of the underlying neural mechanisms.

A remarkable amount of research has also pur-

*Corresponding author.

sued a generalization of common features of retina processing and unification of different retina models [10–18]. However, these are often ad hoc models whose parameters can be modified but not their retina architecture. Generally, their primary goal is to propose a functional model of the whole retina, though, none of the previously cited models can be fully configured to reproduce different physiological experiments than those they have been intentionally designed for.

We present a new framework for computational retina modeling that is based on interconnection of basic processing modules to reproduce different retina behaviors. Our work addresses the following issues with the ultimate purpose of validating, by computational simulations, the hypothesis that a few retinal structures may be repeatedly involved in different retina functions:

- *Computational retinal microcircuits.* There exist sufficient examples of single neural structures that play quite different roles in the retina processing to motivate the generalization of basic retinal building blocks[3]. We implemented a set of computational retinal microcircuits at different abstraction levels that have been recurrently used in the literature for modeling different stages of the retina. We show that different retina models can then be simulated by creating and combining these circuits to form different retina architectures. To the best of our knowledge, this idea, inspired by neural simulators, of computational retinal microcircuits as basic building blocks is a novel concept in retina modeling.
- *Functional and biologically accurate models.* Although we employed more detailed processing microcircuits (e.g., a single-compartment model) in some retina stages to better fit electrophysiological recordings, our main objective was to provide functional models and descriptions as simple as possible to describe the retina phenomena. Moreover, the focus of this framework is on generalizing and summarizing the computational basis of retina modeling, and therefore this premise goes against any specificity in the model description. In spite of the constraints that such an approach raises, we achieved a remarkable level of biological accuracy, comparable to some of the most accurate retina models proposed heretofore [19; 20].
- *Association of every retina stage with a plausible biological mechanism.* Amongst models of retinal processing as a whole, some of them focus on a more functional modeling of every retina stage [10; 12] and other models include some stages that have a stronger relationship to biophysical properties, while some fixed processing behaviors are assumed for the rest[19; 15]. Some of the latter models use multi-state kinetic modules that group together different components of the retina behavior (e.g., fast and slow components of temporal contrast adaptation) and may blur the understanding of the biological mechanisms underlying different retina stages[19]. In contrast, the retina models we developed using the computational retinal microcircuits, connect every retina stage with a plausible biological mechanism in accordance with other authors [11].
- *Retina simulation software interfaced with spiking neural networks.* To provide researchers with a simulation tool that reflects all these concepts, we developed a new software platform for efficient computational retina modeling, called COREM. Computations of spatiotemporal equations performed by retinal microcircuits take advantage of recursive filtering techniques and multithreading. COREM uses a time-driven simulation approach to update functions that describe neuron membrane potential and synaptic currents. An interface with spiking neural network simulators allows generation of the spiking response of ganglion cells. The retina model can be easily loaded in the script of the neural network simulator as an extension module, facilitating its connection to models of higher visual areas, such as the Lateral Geniculate Nucleus (LGN) and the visual cortex.

2. Computational retinal microcircuits

In spite of the wide variety of existing retinal cells (there are more than 50 clearly distinct cell types) some neural circuits are encountered repeatedly in many different retina behaviors[3]. This suggests functionality arises from connectivity of the neural network and not so significantly from features of every individual cell. Moreover, after an extensive review of the literature about retina modeling, we observed that some computational algorithms have been repeatedly used to explain different properties of the retina processing (e.g., a Gaussian filter to character-

ize the receptive field of a cell, as discussed below).

We made a selection of 5 computational microcircuits (Fig. 1) that can be combined to reproduce single-cell and large-scale retina models at different abstraction levels. They can be classified as block-structured models, block-compartment models and single-compartment models according to the scheme proposed by Guo *et al.*[4]. With this set of microcircuits our aim was to summarize the basic principles of the retina modeling and embrace some of the most significant algorithms proposed in the literature, without going into depth on the description of the neural morphology.

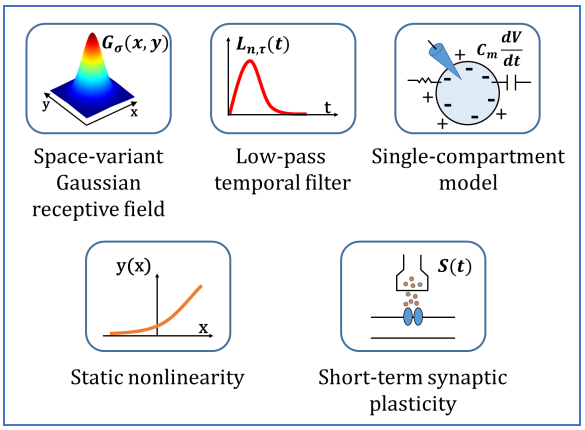

Fig. 1. Computational retinal microcircuits that are used as basic building blocks within COREM. They consist of one spatial processing module, a space-variant Gaussian filter, two temporal modules, a low-pass temporal filter and a single-compartment model, a configurable time-independent nonlinearity and a STP function.

2.1. *Space-variant Gaussian receptive field*

Since the early studies of the cat retinal ganglion cells by Enroth-Cugell [21], the Gaussian filter has become the model of the retinal receptive field par excellence. Sensitivity of the antagonistic center-surround receptive field of ganglion cells is often described by a Difference of two Gaussian kernels, called DOG, with different space constants. However, some cells show a more complex receptive structure than a simple DOG model and different combinations of Gaussian filters are proposed to capture the neural response more accurately[22–24].

At single-cell level, a Gaussian kernel is used to approximate the biophysics of spatial synaptic integration through dendrites of retinal cells and also electrical couplings between neighboring cells. The computational operation underlying these biological mechanisms can be interpreted in terms of a spatial averaging of the neural signal. The mathematical formulation is a two-dimensional isotropic Gaussian filter, $G_\sigma(x, y)$, of space constant σ.

To counterbalance the low density of cells in the periphery of the retina, the receptive field of cells increases with eccentricity. This retina property is modeled by a space-variant Gaussian filtering scheme that gradually blurs out details as the radial distance to the fovea increases (as shown in Fig. 2).

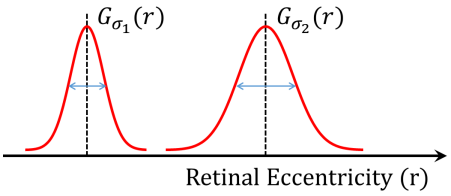

Fig. 2. Increase in kernel size of the Gaussian filter that simulates the change of the receptive field with eccentricity. Coefficients are recurrently computed at each pixel by using a Deriche's recursive filtering adapted to the space-variant case by Tan *et al.*[25]. Amplitude and phase distortion at the right boundary of the image is fixed by including the algorithmic modification by Triggs *et al.*[26].

The traditional convolution algorithm has to deal with two implementation issues: first, a Gaussian convolution is a computationally expensive operation that critically limits the performance of the simulator and, on the other side, in a space-variant approach the convolution kernel is different at each pixel. Our software performs a Deriche's recursive filtering[27; 28], which approximates the Gaussian kernel, and has been extended to the space-variant case described by Tan *et al.*[25].

Other retina simulators[11] also include a space-variant Deriche's filtering although a second order smoothing function[27] is preferred to reduce the processing time over a more realistic Gaussian approximation. In addition, the inherent amplitude and phase distortion produced by this type of recursive filtering at the right boundary of the image is fixed by embodying the corrected version by Triggs *et al.*[26]. When running the simulation in a multicore computer we also take advantage of the fact that every row and every column of the image are processed independently and can be executed in different threads

to parallelize simulations.

2.2. *Low-pass temporal filters*

Low-pass temporal filters have been often used to model synaptic delays and temporal membrane integration of synaptic currents[29; 15; 20; 30; 11; 31]. The standard equation describing the impulse response of a low-pass filter with time constant τ is:

$$L_\tau(t) = \frac{\exp(-t/\tau)}{\tau} \quad (1)$$

Multiple distributed low-pass stages occur along the retinal pathway. Moreover, some single cells already integrate several low-pass filters. An example is the phototransduction cascade at photoreceptors, which roughly includes three processing stages: the outer segment transduction cascade, inner segment ion channel interactions and interactions in the cone pedicle. A cascade of low-pass filters can be expressed in a compact format:

$$L_{n,\tau}(t) = \frac{(nt)^n \exp(-nt/\tau)}{(n-1)!\tau^{n+1}} \quad (2)$$

If $t > 0$, and zero otherwise (causal filters). Temporal low-pass filters also use a recursive approach. We decided to employ an implementation of temporal filters that is based on the Infinite Impulse Response (IIR) approach by Virtual Retina[11], which requires less memory and calculations than a similar Finite Impulse Response (FIR) filter. In this type of filtering, preceding output values, $Y(k-i)$, are used in the calculation of the new output values, $Y(k)$, at the current time step k:

$$Y(k) = \sum_j b_j X(k-j) - \sum_i a_i Y(k-i) \quad (3)$$

where $X(k-j)$ are the preceding input values. Coefficients a_i and b_j are calculated for each filter according to the equations provided in the above-mentioned publication[11].

2.3. *Single-compartment model*

Single-compartment models such as the classic Hodgkin-Huxley model[32] neglect the neuron's spatial structure and focus entirely on how its various ionic currents modulate the subthreshold response[33]. Thus, spatial description of a neuron is simplified to a point neuron and its membrane potential represented by a single variable, V. The basic equation for a single-compartment model is[34; 35]:

$$C_m \frac{dV(t)}{dt} = \sum_i I_i(t) + \sum_j g_j(t)(E_j - V(t)) \quad (4)$$

where C_m is the membrane capacitance, $I_i(t)$ represent external currents (e.g., electrode currents or synaptic inputs), $g_j(t)$ are conductances of ionic channels (including a leak conductance) and E_j their reversal potentials. Provided that the simulation step Δt is sufficiently small, numerical integration of the single-compartment model is approximated by the Euler method[34; 36]:

$$V(t+\Delta t) = V_\infty + (V(t) - V_\infty)\exp(-\Delta t/\tau_V) \quad (5)$$

with

$$V_\infty = \frac{\sum_j g_j(t)E_j + \sum_i I_i(t)}{\sum_j g_j(t)} \quad (6)$$

and

$$\tau_V = \frac{C_m}{\sum_j g_j(t)} \quad (7)$$

Most of the interesting electrical properties of neurons arise from nonlinearities associated with changes of membrane conductances over time[34]. Models of membrane conductances describe the probability that a channel is in an open, ion-conducting state at any given time. This probability, formulated in terms of gating equations, depends on the time course of membrane potential (for a voltage-dependent conductance), the presence or absence of a neurotransmitter (for a synaptic conductance), or other factors such as the concentration of calcium (for a calcium-dependent conductance).

Our interest in modeling membrane conductances lies in their functional properties to implement intrinsic and inter-cell mechanisms of feedback that allow gain control of the neural signal. Therefore, a rapid increase in the membrane potential of a cell, as an example, would elicit a proportional rise in the value of a voltage-dependent conductance $g_j(t)$, which would produce the consequent decrease of the neural gain $dV(t)/dt$ (Eq. 4). In the same manner, $g_j(t)$ defines the time constant τ_V of the single-compartment model and accounts for adaptive changes of the dynamics in the cell processing (Eq. 7). A gain control serves a dual purpose by adapting the dynamic range of the visual pathway, avoiding response saturation, and protecting the cell from

quick and large synaptic currents that could damage its internal structure.

Besides our implementation, which provides a description of this feedback mechanism based on changes in membrane conductances, many other retina models also use a feedback component to explain neural gain control in early stages of the visual system. This mechanism is sometimes also called shunting inhibition, divisive feedback or neural normalization[37]. There are several models that reproduce the phenomenon of contrast gain control in the retina[38; 11; 15], LGN[39], and primary visual cortex[40]. Other models also include a feedback loop to simulate adaptation to the mean light intensity[41; 20] or directional selectivity to motion [42; 43]. We can also find models in silicon of gain controls that reproduce wide-field motion-sensitive neurons[44].

2.4. *Static nonlinearity*

Some common time-independent transformations of the neural signal, such as polynomial, rectification or sigmoidal transformations (Fig. 3), are accounted for by a configurable static nonlinearity. A static nonlinearity captures the input-output relationship between synaptic input of a neuron and its postsynaptic response. They are used to introduce some important signal corrections performed by neurons (e.g., thresholds and saturation) into accurate estimates of neural responses[34; 45].

A static nonlinearity is one of the two different processing stages described by the well-known Linear-Nonlinear (LN) analysis[46–50]. In this scheme, the input stimulus is convolved with a linear temporal filter and the result is transformed by a static nonlinearity to the neuron's response. The linear filter represents the temporal relationship between the stimulus and the neuron's response, whereas the nonlinearity represents the instantaneous mapping between the filtered stimulus and the response.

Within the different transformations implemented, a rectification function prevents the predicted neural response (and the firing rate in the case of ganglion cells) from becoming negative:

$$y_{x>thr}(x) = ax + c \tag{8}$$

If needed, a saturating nonlinearity can be included, and a sigmoidal function is often used for this purpose:

$$y(x) = \frac{b}{1 + \exp(-ax + c)} \tag{9}$$

Other polynomial transformations, used to model, for example, convex functions of a contrast feedback mechanism[11], are defined by:

$$y(x) = ax^b + c \tag{10}$$

in which, a, b and c are configurable parameters that can be tuned to fit a specific neural transformation.

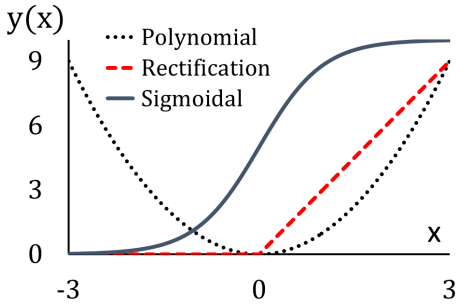

Fig. 3. Functions that represent the main nonlinearities that can be configured in COREM: polynomial, rectification and sigmoidal (apart from the other two nonlinearities not cited in the text but also implemented: threshold function and a piecewise function). Parameters of these functions and x values have been arbitrarily chosen to provide a graphical example.

2.5. *Dynamic nonlinearity with short-term synaptic plasticity*

Short-term plasticity (STP) refers to a phenomenon in which synaptic strength changes over time in a way that reflects the history of presynaptic activity and it lasts from milliseconds to tens of seconds[51; 34; 52]. There are two types of STP, with opposite effects on synaptic efficacy, which are known as short-term depression and short-term facilitation. The main type of adaptation observed in the retina is depression (although another forms of plasticity are also reported[31]) and it is caused by depletion of neurotransmitter release when a strong input stimulus is maintained over time.

Our main motivation to implement a plasticity microcircuit lies in recent findings hypothesizing that depression at the bipolar-to-ganglion cell's synapse is responsible for retinal adaptation to contrast[53–55] and object motion[56]. We propose a STP function

that modulates the baseline of the bipolar cell's output response, at the bipolar-to-ganglion cell's synapse. It mainly affects the static nonlinearity of the LN analysis by shifting its offset and accounts for the two different forms of adaptation studied for contrast and object motion, fast (smaller than 100 ms) and slow (in the range of a few seconds).

To reproduce fast adaptation timescale, our STP model implements a simple updating rule based on cell's presynaptic activity, which is used in spiking network models and has been adapted to the analog neural processing of the retina[34]. Assuming the input function is normalized to have zero mean, the offset $S(t)$ is continuously augmented an amount proportional to the variance of the input:

$$S(t) = S(t) + k_f(k_s(t)|input(t)| - S(t)) \quad (11)$$

where k_f is a parameter that specifies the fast adaptation rate and $k_s(t)|input(t)|$, with $k_s(t)$ the slow adaptation term (explained below), limits the maximum value the offset can reach. The term $|input(t)|$ provides a rectified measure of the input synaptic activity.

Over the period of slow adaptation, the baseline shows an exponential decay and recovery for steady input patterns of high and low contrast respectively[48; 55; 57]. The slow recovery of the membrane offset following high contrast stimulation is often called prolonged membrane after-hyperpolarization (AHP). Synaptic depression explains slow adaptation, not only in the retina but also in the visual cortex[58; 59]. We adapted the basic first-order differential equation that is widely used in neural dynamics to describe transitions between different neural states (e.g., active and inactivated states in the four-state system by Ozuysal and Baccus[19]). Slow system transitions during prolonged periods of low and high contrast are governed then by the following equation:

$$k_s(t + \Delta t) = k_\infty(t) + (k_s(t) - k_\infty(t)) \exp(-\Delta t/\tau_s) \quad (12)$$

where τ_s is the temporal constant of the slow adaptation mechanism and $k_\infty(t)$ is inversely modulated by the input activity scaled by a plasticity factor k_d:

$$k_\infty(t) = \frac{k_d}{|input(t)|} \quad (13)$$

3. Overview of COREM

The retinal microcircuits described above are implemented in COREM, a configurable C++ retina simulation software. Our two goals when designing COREM have been to provide scientists with a rapid prototyping tool for retina modeling, which facilitates the study of low-level visual mechanisms, and to optimize efficiency of all its modules. An example of this optimization effort is reflected in computations of spatiotemporal equations performed by the space-variant Gaussian receptive field and the low-pass temporal filter. Both modules are formulated as recursive filters and, besides, we employ OpenMP to gain thread-level parallelism in the Gaussian filter (see Section 2 for further details). On the other hand, unlike a conventional neural simulator, layers of neurons in the retina are handled as images (using CImg library[60]), with all the benefits that this entails, such as simultaneous access to internal variables of multiple neurons in a SIMD processor.

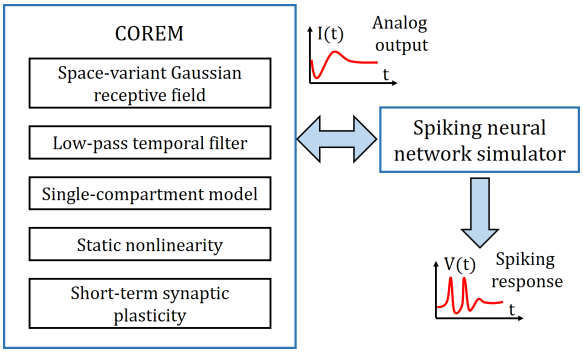

Fig. 4. Interface of COREM with a spiking neural network simulator. While COREM sends data of the analog presynaptic current of ganglion cells, the ganglionar spiking response is reproduced by the spiking neural network simulator.

The modular structure of COREM allows for more flexibility of use than other retina simulators[10; 11]. The user can create and connect any number of computational retinal microcircuits by configuring a simulation script that follows a similar syntactic structure of the neural simulator scripts. Computational retinal microcircuits do not represent specific neuron types but rather basic retina operations that can be combined to reproduce the behavior of single neurons or networks of neurons. We formulated these units in this manner to endow the simulation software with a higher configurability

that allows implementation of different retina models. Moreover, built-in tools for visual stimulation and data analysis give the possibility to reproduce some of the most common experimental setups used in electrophysiology of the retina (e.g., sinusoidal drifting gratings or uniform white flashes). Visual stimulus functions, as well as methods for data analysis, were implemented according to the descriptions given in publications referenced in Section 4.

Equations of neuron dynamics are updated in a time-driven fashion consistent with the analog processing architecture inherent to the retina. COREM does not provide retinal microcircuits to explicitly generate the spiking response of ganglion cells. Instead, an interface with spiking neural network simulators allows bidirectional communication with them to simulate firing mechanisms (see Figure 4). Thus, when connecting COREM with a spiking neural network simulator, simulation is driven by the latter one, which periodically sends update requests and receives data of the analog presynaptic current of ganglion cells. Ganglion cells can be simulated as simple integrate-and-fire or more complex models of spiking neurons[62] in the neural network simulator. Integration with models of higher visual areas is therefore carried out by simply instantiating COREM as an extension module in the script of the neural network simulator.

4. Simulation results of electrophysiological experiments

To show the potential of the proposed framework, we constructed three different retina models that describe some well-known properties of the retina processing (see Figure 5), and we fitted them to published electrophysiological recordings. Our contribution in this aspect has been to adapt and combine some representative models proposed in the literature so that they can be implemented using the computational microcircuits described in Section 2.

Consistent with the premise of repeatability in the retina processing pathway[3], our retina models comprise some processing steps that are common to all of them. For example, a divisive feedback loop is present in many stages of different models, such as the inner segment of the cell's model for adaptation to the mean light intensity in Figure 5A, and bipolar cells of the contrast gain control shown in Figure 5B.

Inspired by the numerous approaches that have been proposed for describing the different retina functions, these retina models provide a simple but biologically realistic description of the retina processing. We wanted them to be sufficiently representative and general with the aim of including most of the concepts that characterize retina computations.

4.1. *Adaptation to the mean light intensity*

The visual system routinely copes with the problem of processing the high dynamic range of light intensities in natural environments by regulating sensitivity to light at early stages of visual processing. This dynamic range is obtained mainly by gain control mechanisms that adjust the cell's dynamics to the steady illumination level. Although post-receptor adaptation has been also reported, the outer retina is suggested to be the major locus for adaptation to the mean light intensity[30; 63; 64]. We simplified and adapted the molecular model of cones and horizontal cells proposed by van Hateren[20] to fit electrophysiological data obtained from horizontal cells of the macaque retina[30].

4.1.1. *Model of cones and horizontal cells*

Figure 5A shows a model of the cone photoreceptor, which comprises the outer segment (phototransduction and calcium feedback) and the inner segment, coupled to a horizontal cell's feedback mechanism. The first stage reproduces the temporal low-pass filtering followed by a static nonlinearity of phototransduction by cones. A cascade of first-order low-pass filters is commonly used as initial stage in different models of retinal light adaptation to approximate the retina response when the mean light level is low[65; 41; 30; 66]. In other words, this initial low-pass filtering is the low-light limit of the temporal frequency response.

By contrast, when the mean light level increases, gain at low frequencies is inversely proportional to the mean light level. Divisive feedback[20; 65; 41] and feedforward[67; 63] gain controls have been proposed to shape this adaptation phenomenon. Some authors noted that feedback gain controls tend to be too slow to account for measured cell's response[63]. However, it was demonstrated that an inhibitory feedback split into three stages, calcium feedback, inner segment and horizontal cell's feedback, gives a remarkable

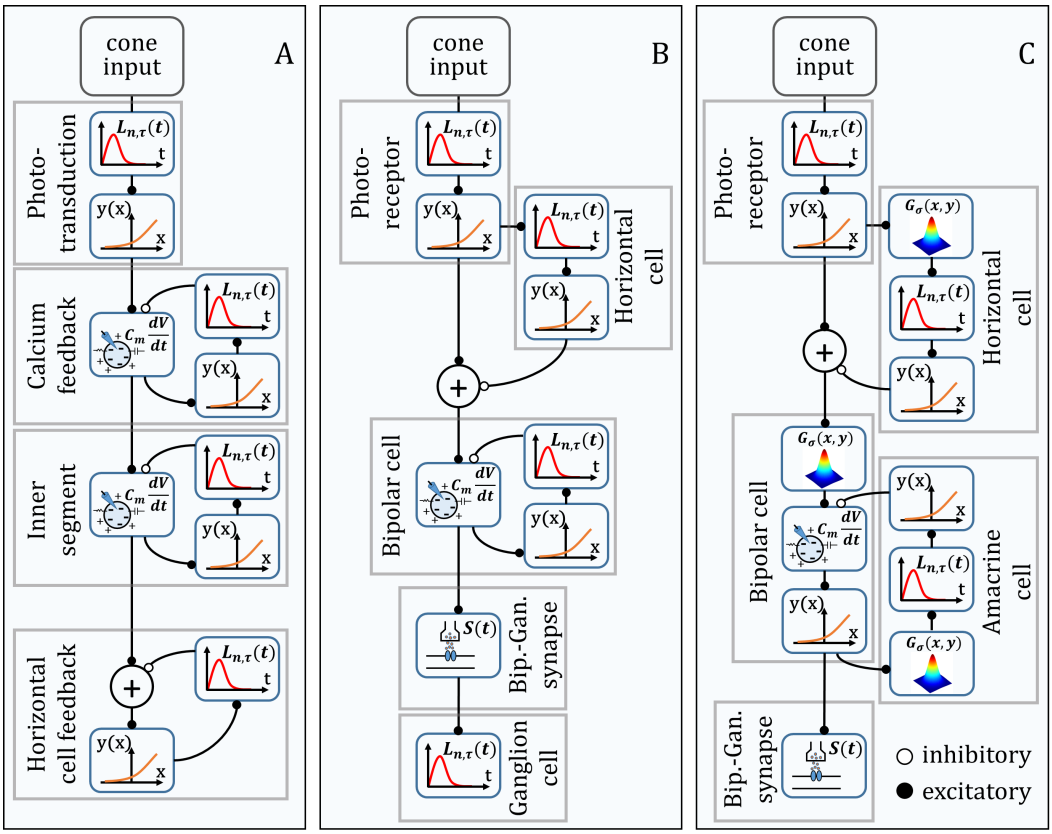

Fig. 5. Retina models implemented by connection of the retinal microcircuits described in Section 2. They reproduce adaptation to the mean light intensity (A) and to temporal contrast (B), and differential motion sensitivity (C). Interconnections are either sign preserving (excitatory, black circles) or sign inverting (inhibitory, white circles). A circle with the plus sign (+) represents linear addition of neural signals. Feedback mechanisms formed by a single-compartment model, a static nonlinearity and a low-pass temporal filter connect the input from the preceding retina stage to the current port ($I_i(t)$ in Eq. 4) and the feedback branch to the conductance port ($g_j(t)$ in Eq. 4). Thus, conductance of the single-compartment model is modulated by the feedback signal. Cone inputs correspond to the transformation that maps the input visual stimuli to the cone spectral sensitivities by using the Hunt-Pointer-Estevez (HPE) matrix [61]. For these experiments, the type of cone (L, M or S) is not specified because a spatially uniform achromatic stimulus is employed.

good fitting and better reflects the inherent biology of photoreceptors and horizontal cells[20].

While formal definition of some of the different feedback loops proposed in our retina models includes a calcium-dependent mechanism (e.g., the calcium feedback in the model presented here or the intrinsic adaptive mechanism at bipolar cell level in Figure 5B), we have implemented them using a single-compartment model and a feedback conductance that resembles a voltage-gated conductance. Calcium- and voltage-dependent conductances can be roughly described by the same set of equations, although physiological interpretation of their parameters is different[34; 35]. In a calcium-dependent system, the adaptive conductance would depend on the concentration of calcium inside the neuron instead of a direct relationship with its membrane potential. Calcium-activated channels are opened by increases in concentration of intracellular calcium occurring during synaptic transmission. Thus, a rise of calcium influx produces an increase of the calcium-dependent conductance that feedbacks the current neural state and results in a similar gain control of the neural system.

In the model, the calcium feedback pathway consists of a low-pass filter with a small time constant (5 ms) and a polynomial static nonlinearity that modulates strong feedback by using an exponent of value 4 (both time constant and exponent values are comparable to τ_c and n_c in the model by van Hateren[20]).

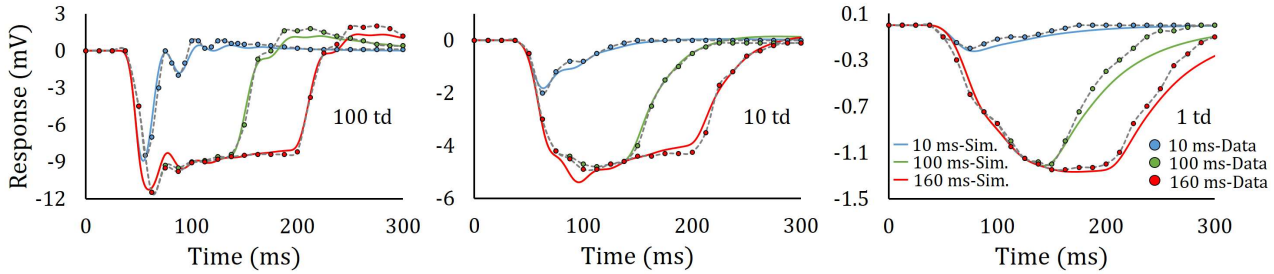

Fig. 6. Simulation results for the model of adaptation to the mean light intensity (color solid lines) and electrophysiological recordings (color markers) obtained from horizontal cells of the macaque retina[30]. Data points have been sampled from Figure 6 in the publication[30]. Input stimuli are spatially uniform white pulses of 10, 100, and 160 ms at a fixed Weber contrast of 8 and background illuminances of 1, 10 and 100 trolands. All pulses start at 0 ms. A gray dashed line has been used to interpolate electrophysiological data and improve visualization.

Much of the adaptation process is rapidly driven by the calcium feedback, which is mainly responsible for reducing the response gain. The inner segment feedback has a higher time constant and an exponent of value 2 to follow up finer adaptation features (e.g., resonant oscillations in the impulse response, represented in Fig. 6). A linear subtractive scheme is used for the horizontal feedback shown in the last stage of Figure 5A.

While modeling similar feedback architectures for the inner segment and horizontal cells, we have largely simplified the circuitry proposed by van Hateren[20] and slightly modified their roles in the adaptation process. A divisive feedback loop, such as the inner segment feedback, can be easily tuned to produce high-frequency oscillations, which represents a simpler design approach. On the other hand, a linear subtractive scheme at the horizontal cell's level, which doesn't include complex nonlinear components, is consistent with the slow linear inhibition performed by horizontal cells and implemented also in the rest of retina models.

4.1.2. *Responses to pulses*

Figure 6 shows simulated and measured responses to uniform white pulses of 10, 100, and 160 ms at a fixed Weber contrast of 8 and background illuminances of 1, 10 and 100 trolands (td). The model fittings (red, green and blue solid lines) were made to all stimulus conditions simultaneously, and are generally quite good approximations, considering the wide range of stimulus conditions. Details of multiobjective parameter fitting of the model are given in appendix A.

It is possible to identify the main stages of the model responsible for various aspects of the response shapes. The calcium feedback plays a key role in gain control, preventing the response from scaling proportionally with the background luminance. It may be noted that high-frequency oscillations due to the inner segment feedback, shown at the onset and removal of the stimulus, are more prominent for a 100 td background and nearly imperceptible for the 1 td background. At low mean light intensities the inner segment cannot produce a strong feedback and its effects are less prominent, compared to the previous stage, because of the lower value of the exponent in the static nonlinearity. Slow decrease in the steady response and rebounds after stimulus removal are motivated by the linear horizontal cell's feedback.

4.1.3. *Responses to sinusoidal gratings*

By using the same model parameters of the previous experiment, a new stimulus is simulated to represent sensitivity as a function of frequency and background illuminance (see Figure 7). For each background illuminance, temporal frequency of a low-contrast sinusoidal grating, at three different background illuminances (10, 100 and 1000 td) is progressively increased and the response amplitude divided by the background illuminance to calculate sensitivity (in mV/td) at different frequencies.

The model captures the main features of the experimentally measured response[30] and simulated responses resemble those obtained in other models[20]: a decrease of responsivity as a function of the background level for low frequencies, and asymptotic convergence at high frequencies; an increase of the cut-off frequency as a function of background level; and

a resonance peak at higher frequencies, particularly visible at the 100 and 1000 td background levels.

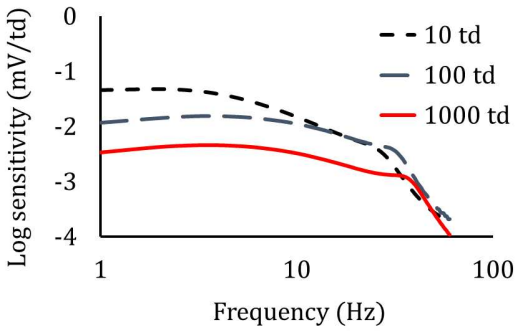

Fig. 7. Logarithm of the amplitude sensitivity of the simulated model (in mV/td) plotted as a function of the grating frequency for different background illuminances (10, 100 and 1000 td). Physiological recordings are not included in this figure because authors[30] do not provide an averaged inter-cell response that could be used as optimization target. Our results reproduce remarkably well all features of the neural behavior (e.g., cutoff frequency) and simulated values are within the range of measured values for the different cells.

4.2. *Fast and slow temporal contrast adaptation*

Adaptation to the variance of light intensities is known as temporal contrast adaptation. After a change in contrast, retinal cells express at least two adaptive mechanisms: a fast change in the response occurs within the first tens of milliseconds and a slow component over some tens of seconds following the contrast switch[48; 46; 68]. When the stimulus environment changes from a low to high variance, temporal filtering quickly accelerates, sensitivity decreases, and the average response increases. For a high-contrast pattern maintained over time, a slow decay in the average response is produced that opposes the fast change in the cell's baseline. Upon a decrease in contrast, all these changes reverse direction. The time constants for slow adaptation are asymmetric, with the baseline decaying faster in high contrast than it rises in low contrast[48; 19].

Contrast adaptation originates in bipolar cells and neither photoreceptors nor horizontal cells are involved in the process [69; 46]. Some experiments have shown that contrast adaptation effects are still present under physiological blockade of amacrine synapses, ruling out a critical role for amacrine cells in driving contrast adaptation [69; 47]. Slow adaptation mechanisms are apparently driven by prolonged reduction of glutamate release at the bipolar-to-ganglion synapse[53–55]. Gain of spike generation at the level of ganglion cells adapts to contrast by slow inactivation of voltage-dependent Na^+ channels[70; 48]. Recordings in bipolar cells suggested that another intrinsic gain control mechanism lies in the bipolar cell dendrites and depends on calcium feedback[47; 54].

Our goal was to accurately predict intracellular recordings of ganglion cell's membrane potential[19] by capturing all adaptive features of temporal filtering and the static nonlinearity in the LN analysis. Gain control in the subthreshold response of ganglion cells originates from gain control of its excitatory bipolar cell inputs[69]. We implemented an intrinsic mechanism for gain control at the level of bipolar cells, which can account for most of the fast-onset contrast adaptation[46; 47], and another mechanism of STP at the bipolar-to-ganglion synapse[55].

4.2.1. *Retina model*

Figure 5B shows a whole retina model that accounts for fast and slow contrast gain control. The first stage is a linear subtraction at the Outer Plexiform Layer (OPL) to represent the well-known opposition between the center of the receptive field, driven by photoreceptors, and the surround signal transmitted by horizontal cells. In the time domain, a biphasic impulse response results from subtraction of photoreceptor signal and its delayed version by horizontal cells, and this is the characteristic temporal shape observed throughout all retina stages. We decided to implement this OPL model, rather than using a predefined linear filter[19], because each of its components has direct connection with biological mechanisms. Note that the center-surround structure at OPL is repeated for the other retina models in Figure 5 but including spatial filtering modules (i.e., Gaussian filters) that have been omitted here since they are not relevant for the processing of a spatially uniform stimulus.

Bipolar cells implement a contrast gain control based on a divisive feedback loop[11; 39; 15; 38] and may be associated with the calcium-dependent mech-

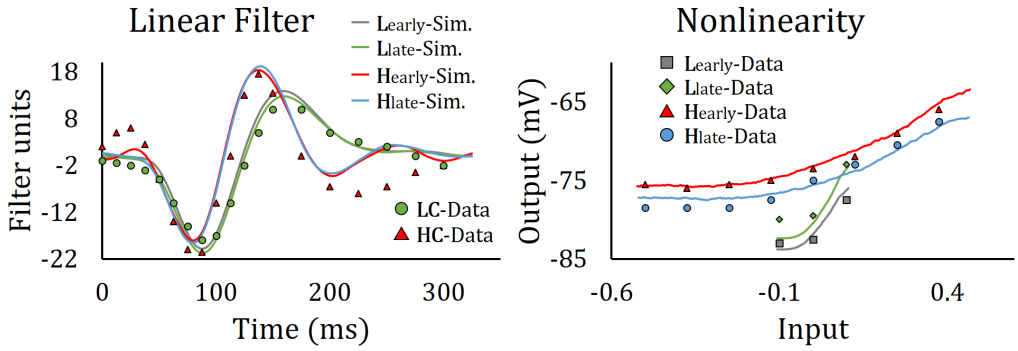

Fig. 8. LN analysis of the simulated response of the model for contrast adaptation (solid lines) fit to intracellular recordings (color markers) of salamander ganglion cells[19]. Data points have been sampled from Figure 3 in the publication[19]. Four different contrast intervals are considered in the average of measurements: L_{early} corresponds to the first 10 seconds after a low contrast step and L_{late} to the period from 10 to 20 seconds after a low contrast step. H_{early} and H_{late} are defined similarly for a high contrast step. LC refers indistinctly to L_{early} and L_{late}. Similarly for HC. They are used in the linear filter because measured curves over the contrast periods are identical. The input stimulus is an alternating spatially uniform sequence of high and low contrast periods of 20 s. Values of the sequence are chosen every 5 ms, which corresponds to the simulation step, from a Gaussian probability distribution with normalized mean intensity 0.5. Contrast, defined as the quotient between standard deviation and mean intensity of the Gaussian distribution, was 0.1 for low contrast patterns and 0.5 for high contrast patterns. We have followed the correlation method described by Baccus and Meister[46] to generate results of the LN analysis.

anism observed in the bipolar cell dendrites[47]. Neural state of bipolar cells is driven by the local measure of contrast provided by the OPL signal. The feedback pathway rectifies and amplifies the current neural signal of bipolar cells to continuously modify an adaptive conductance of the single-compartment model, in a similar manner to other approaches for contrast adaptation[11; 39]. An increase of the adaptive conductance has the double effect on bipolar cells of reducing its neural gain $dV(t)/dt$ (Eq. 4) and decreasing the temporal constant τ_V (Eq. 7). Thus, a stimulus switch to high contrast decreases sensitivity and accelerates temporal filtering of bipolar cells.

Most of retina models for contrast gain control do not reproduce all adaptive features of the static nonlinearity in the LN anlysis[11; 39; 38; 15]. By introducing a STP at the bipolar synaptic terminal our goal was to reproduce offset changes in the bipolar cell's response. The main effects that are modeled by the STP module are a fast increase in the response to the onset of high contrast adaptation, slow decay of the response for a maintained high-contrast pattern and the consequent membrane AHP recovery afterwards.

4.2.2. *LN analysis of ganglion cell's membrane potential*

Figure 8 compares the LN analysis of simulation results and intracellular recordings of salamander ganglion cells[19]. We have presented results of a preliminary version of this retina model in Ref. 71, 72. Here, parameters of the model in Figure 5B have been optimized for fitting simultaneously to both the linear filter and the static nonlinearity (see appendix A). The model captures fast adaptation changes in the temporal filter: a high contrast step decreases the time to peak with a consequent acceleration of the neural dynamics, and makes the temporal response more differentiating. Fast adaptation changes are also observed in the static nonlinearity by a decrease of the sensitivity, which is defined as the average slope of the nonlinearity, and a quick depolarizing offset, as measured by the increase of the average value. Slow adaptation mainly affects the offset of the static nonlinearity, by decreasing it during a high contrast period and motivating its slow recovery after a switch to low contrast (Figure 9).

Experimentally we observed that gain control at bipolar cells can be understood as a push-pull mechanism between the OPL biphasic signal and feedback response. A weak feedback would result in a perfect

fit of the OPL biphasic shape (characterized by the first negative peak and maximum value of the linear filter within the first 150 ms in Figure 9) and a complete removal of the second minimum reflected in the measured data (after 200 ms). By contrast, an increase in the feedback signal would worsen approximation of the first negative peak and pull the response after 150 ms towards this second minimum. Since both minimum values of the linear filter cannot be perfectly fit simultaneously we present a trade-off solution by a multiobjective optimization that slightly deviates from measures of late values in the high-contrast curve but produces a fairly well fitting of the rest of curves.

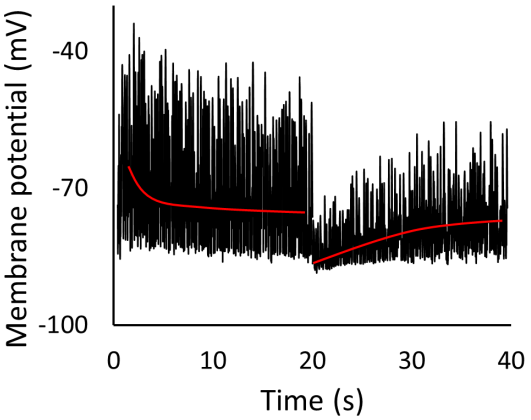

Fig. 9. Simulated membrane potential of ganglion cells over time. In this figure, the first 20 s correspond to a high contrast period and the following 20 s to a low contrast period. The red solid line approximates the offset of the neural response. The contribution of two distinct temporal components, fast and slow, to the onset of high contrast adaptation is suggested by asymmetric time courses of the different contrast periods. Fast adaptation changes are more significant for an increase in contrast, which results in a peak of the membrane potential after a contrast switch (at 0 s). A slow decay in the membrane potential is produced afterwards. By contrast, when a low contrast step occurs (at 20 s), AHP restores the baseline and opposes previous changes. This figure has been adapted from Figure 3 in a previous publication[71].

One of the most detailed retina models for contrast adaption, which also reproduces all adaptive features, has been proposed by Ozuysal and Baccus[19]. In their model, the late values of the high-contrast are approximated by a flat response of the system (Figure 3 of the publication[19]), whereas our model shows somehow a tendency to reproduce this rebound of the measured neural response. Strong oscillations of the high contrast curve do not represent the neural response of all cells measured but they often appear in cells that strongly adapt to contrast[73; 46]. We could hypothesize that another adaptive mechanism (e.g., a second feedback stage with different time constants), which activates for high contrast stimuli, could account for this negative rebound.

4.3. *Object motion sensitive (OMS) cells*

The visual task of detecting objects moving within a scene is not a trivial task. Image motion on the retina can be produced by two different reasons. One is the movement of objects in the scene. The other results from self-motion, such as translation when walking or movements of the head, and eye movements, large gaze-shifting eye movements and the incessant fixational eye movements.

To detect moving objects, a type of ganglion cells, referred as object motion sensitive cells (OMS), distinguish differential motion, between the receptive field center and surround, from the global retinal image drift[74; 56; 75]. An OMS ganglion cell remains silent under global motion of the entire image but fires when the image patch in its receptive field moves differently from the background. To accommodate all kinds of observer motion, this selectivity for differential motion does not depend on direction of motion, nor the image pattern, only on the speed.

4.3.1. *Retina model*

Our retina model (Figure 5C) is a computational implementation of previous models[74; 75] that includes as a novelty the STP microcircuit at the ganglion cell's synaptic input to produce differential motion adaptation. In this model, ganglion cells pool neural signals within its receptive field from many retinal structures formed by the bipolar cell's processing pipeline shown in Figure 5C (the Gaussian filter at ganglion cell's synapse is not represented in this figure). One can identify two key components that modulate the OPL biphasic response from photoreceptors and horizontal cells and account for differential motion detection in the subthreshold response of ganglion cells. The first one is formed by spatial pooling of rectified responses of bipolar cells. It ex-

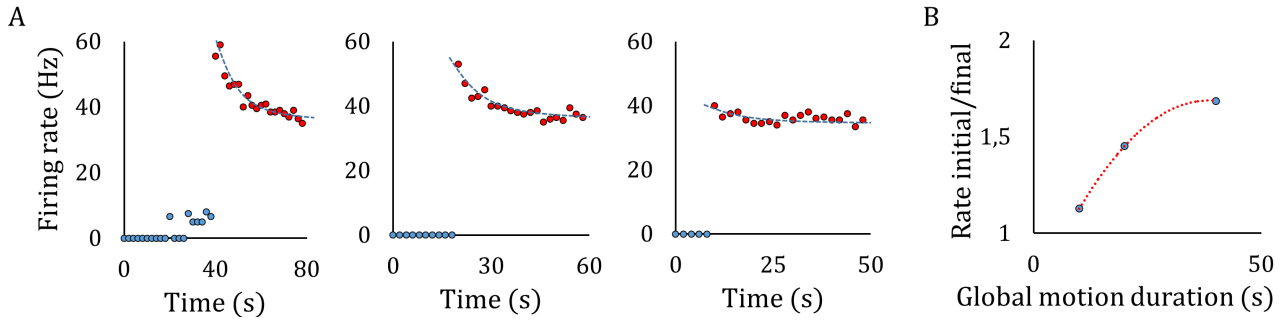

Fig. 10. (A) Simulated firing rates of OMS cells in response to a jittering grating alternating between 40 s of differential motion (red markers) and a varying interval of global motion (blue markers). A dashed blue line interpolates simulated values for the differential motion interval. Global motion corresponds to the first 40 s in the first graph, 20 s in the second and 10 s in the last graph. (B) Firing rate at the onset of differential motion divided by the final value of this interval, plotted as a function of the preceding duration of global motion (B). The jittered gratings consisted of black and white bars with a spatial periodicity of 0.57 degrees of retina visual angle. The object region (a circle) was 1.14 degrees in diameter and the whole retina surface simulated encompassed 5.7 degrees. The jitter trajectory was generated by stepping the background and object gratings periodically in 1D every 15 ms with a step size of 0.029 degrees, synchronously for global motion and asynchronously for differential motion. The retina model is connected with NEST[6] to simulate leaky integrate-and-fire ganglion cells and generate the spike train data. Parameters of the model have been tuned manually to approximate the neural behavior, assuming firing rates which would be registered for a single trial, of Figure 2 in the publication by Ölveczky *et al.*[56].

plains the fact that OMS cells respond to gratings much finer than the receptive field center, and independently of the phase of the grating[76].

The second important computational property of the OMS circuit arises in this model from background inhibition, possibly driven by polyaxonal amacrine cells, of the central region of the ganglion receptive field. Both the excitatory signal from bipolar cells and inhibition from amacrine cells are delivered to ganglion cells in a sparse sequence of transient pulses, which correlate with shifts of a jittering motion stimulus. Thus, if the background trajectory matches the object trajectory in the center of the receptive field, inhibition and excitation synchronize and the OMS ganglion cell remains silent.

The retina model adds a STP microcircuit at the synapse from bipolar to ganglion cell. Based on the same concept of slow contrast adaptation discussed above, the STP microcircuit reproduces differential motion adaptation by synaptic depression. Therefore, during continued exposure to differential motion, the firing rate of OMS cells exponentially decreases with average time constants in the range 2-20 s[56]. A similar asymmetry is also found in time constants of global and differential motion adaptation. Recovery from differential motion adaptation occurs more slowly, with an average time constant of 52 s.

4.3.2. *Recovery from differential motion adaptation*

A jittering grating has been used to reproduce the experimental setup that simulates fixational eye movements[74; 56; 75]. This grating stimulus divides the image region into an object region covering mainly the ganglion cells receptive field center and a peripheral large background region covering the rest of the retina. Both the background and the object gratings jittered periodically with the same statistics, either coherently (global motion), simulating a stationary background scanned by eye movements, or with different trajectories (differential motion).

Figure 10A shows firing rates of OMS cells in response to this stimulus alternating between 40 s of differential motion and a varying interval of global motion. Our simulation results reproduce the neural tendency of cells registered by Ölveczky *et al.*[56]: slow exponential decay for differential motion and changes in the onset of differential motion after different intervals of global motion. The OMS response at the onset of differential motion presents its maximum value when the time interval of global motion is closer to the average time constant of 52 s and the neuron has enough time to recover its membrane baseline (Figure 10B). Longer intervals of global mo-

tion do not significantly increase the OMS response at the onset of differential motion.

5. Conclusions

We have presented a new framework for realistic computational retina modeling that is based on three main contributions: definition of a set of computational retinal microcircuits that can be used as basic building blocks, use thereof to develop retina models that reproduce some of the most characteristic retina functionalities, and implementation of an efficient and configurable retina simulation tool called COREM.

Parameters of the different retina models were optimized to fit published electrophysiological recordings. Our model of photoreceptors and horizontal cells reproduce adaptation to the mean light intensity in response to uniform white pulses at different Weber contrasts, background luminances and as a function of the stimulus drifting frequency. A different retina model accurately predicts temporal contrast adaptation by capturing all adaptive features of temporal filtering and the static nonlinearity in the LN analysis. Finally, we also fitted the neural behavior of OMS ganglion cells for a jittering stimulus that approximates fixational eye movements.

On the other side, we have already published preliminary results[77] of models that implement different retina architectures in the red-green pathway. A retina circuit that reproduces the coextensive receptive field structure in the blue-yellow pathway[78] is currently being developed as well. Both models of the chromatic pathways can be implemented in terms of the computational retinal microcircuits. While our retina models fulfill the goal of this study, future work will require validating these models against new physiological data. Model validation will provide us with a measure of how accurate these models are to predict outcome values for previously unseen data.

Retina models proposed in the literature are often ad hoc models whose parameters can be modified but not their connection scheme. The modular structure of COREM allows for more flexibility of use than other retina simulators[10; 11]. The user can configure different retina architectures through a simulation script that follows a similar syntactic structure of the neural simulator scripts. Following the example of neural simulators, the computational retinal microcircuits implemented in COREM unify different concepts found in the literature and represent some of the most recurrently used algorithms for retina modeling.

With this framework, we have shown by computational simulations that a single processing structure can be plausibly involved in the processing pathway of different retina behaviors. This goes in line with the evidence (see Ref. 37 for a review) that the brain performs a set of canonical neural computations to solve similar problems across different brain regions. A clear example is the feedback mechanism which we have recurrently used to perform gain control (also called divisive normalization) of the neural signal.

While we now have a good understanding of most of the constituent cell types in the retina and some general ideas of their connectivity, computational operations performed by the retina remain as an open research topic. Unified frameworks of different computational theories proposed for the retina modeling are valuable tools that can facilitate future studies in this area.

Acknowledgments

This work has been supported by the Human Brain Project (FET project 604102), Spanish National Grants TIN2013-47069-P and TIN2012-32039, projects P11-TIC-7983 and P11-TIC-8120 of Junta of Andalucia (Spain), co-financed by the European Regional Development Fund (ERDF), and the Spanish Government PhD scholarship FPU13/01487. We used the supercomputer Alhambra of University of Granada for parallel processing of the genetic algorithm optimization.

Appendix A Multiobjective parameter fitting

A multiobjective genetic algorithm automatically optimizes parameters of the retina models for adaptation to the mean light intensity and temporal contrast. A general evolutionary search was configured whereby the random initial population of solutions is evolved by applying uniform crossover and Gaussian mutation operators in combination with a well-known multiobjective selection algorithm (NSGA-II[79]).

Different error functions have been proposed to optimize parameters of neuron models and for model

assessment[80–82]. We can distinguish three types of error functions commonly used in neuron model optimization: feature-based, point-by-point comparison of voltage traces and multi-objective functions. To fit the temporal response of our models, we employ a multiobjective function that combines two type of metrics based on point-by-point comparison of voltage traces, the normalized root-mean-square error (NRMSE) and a shape error descriptor.

The first error metric, the (NRMSE) is used to estimate the scale distance between simulated values (y_i) and physiological values (x_i):

$$NRMSE = \frac{\sqrt{\sum_i (y_i - x_i)^2 / n}}{y_{max} - y_{min}} \quad \text{(A.1)}$$

for vectors of length n. A second error metric, which computes the shape error, is based on local measures of angles between line segments of the simulated curve (v_1) and physiological results (v_2):

$$angle_j(v_1, v_2) = arccosine\left(\frac{v_1 \cdot v_2}{\|v_1\|\|v_2\|}\right)/\pi \quad \text{(A.2)}$$

where j is the number of segments. Thus, the first fitness function evaluated by NSGA-II accumulates the NRMSE for the k responses to optimize simultaneously:

$$fitness_1 = \sum_k (NRMSE_k) \quad \text{(A.3)}$$

A regularization term is also included, as a second fitness function, to account for shape errors between simulated and physiological results, which are determinant, for instance, in the response oscillations shown in Figure 6:

$$fitness_2 = \sum_k (shape_k) \quad \text{(A.4)}$$

where $shape_k$ is an algorithm that computes the sum of the angular errors (according to Eq. A.2) for all segments of the curve k.

Appendix B Model parameters

Best fits of parameters found for the different retina models are shown below.

- *Adaptation to the mean light intensity:* $\tau_{photo} = 20.0$ *ms*, $n_{photo} = 2.0$, $a_{photo} = -0.1$, $b_{photo} = 1.0$, $c_{photo} = 0.0$, $C_{calcium} = 1.0\ \mu F/cm^2$, $E_{calcium} = 0.0$, $\tau_{calcium} = 5.0$ *ms*, $n_{calcium} = 2.0$, $a_{calcium} = 1.5$, $b_{calcium} = 4.0$, $c_{calcium} = -1.0$, $C_{inner} = 1.0\ \mu F/cm^2$, $E_{inner} = 0.0$, $\tau_{inner} = 10.0$ *ms*, $n_{inner} = 3.0$, $a_{inner} = 1000.0$, $b_{inner} = 2.0$, $c_{inner} = -2.0$, $threshold_{inner} = -0.1$, $\tau_{horizontal} = 55.0$ *ms*, $n_{horizontal} = 1.0$, $a_{horizontal} = 230.0$, $b_{horizontal} = 20.0$, $c_{horizontal} = 4.0$.
- *Fast and slow temporal contrast adaptation:* $\tau_{photo} = 75.7$ *ms*, $n_{photo} = 9.7$, $a_{photo} = -1.0$, $b_{photo} = 1.0$, $c_{photo} = 0.0$, $\tau_{horizontal} = 45.5$ *ms*, $n_{horizontal} = 6.4$, $a_{horizontal} = 1.0$, $b_{horizontal} = 1.0$, $c_{horizontal} = 0.83$, $C_{bipolar} = 1.2\ \mu F/cm^2$, $E_{bipolar} = 0.0$, $a_{bipolar} = 66.8$, $b_{bipolar} = 1.0$, $c_{bipolar} = 4.2$, $\tau_{feedback} = 31.0$ *ms*, $n_{feedback} = 5.0$, $a_{feedback} = 70.8$, $b_{feedback} = 2.0$, $c_{ganglion} = 6.6$, $a_{ganglion} = 0.5$, $b_{ganglion} = 1.0$, $c_{ganglion} = -95.0$, $k_{(f)ganglion} = 0.5$, $\tau_{(s)ganglion} = 12000$ *ms*, $k_{(d)ganglion} = 6.0$.
- *Object motion sensitive (OMS) cells:* $\tau_{photo} = 30.0$ *ms*, $n_{photo} = 5.0$, $a_{photo} = -1.0$, $b_{photo} = 1.0$, $c_{photo} = 0.0$, $\tau_{horizontal} = 20.0$ *ms*, $n_{horizontal} = 10.0$, $a_{horizontal} = 1.0$, $b_{horizontal} = 1.0$, $c_{horizontal} = 0.0$, $\sigma_{horizontal} = 0.05°$, $C_{bipolar} = 1.0\ \mu F/cm^2$, $E_{bipolar} = 0.0$, $a_{bipolar} = 10.0$, $b_{bipolar} = 1.0$, $c_{bipolar} = 0.0$, $threshold_{bipolar} = 0.0$, $\sigma_{bipolar} = 0.05°$, $\tau_{amacrine} = 5.0$ *ms*, $n_{amacrine} = 0.0$, $a_{amacrine} = 30.0$, $b_{amacrine} = 2.0$, $c_{amacrine} = 2.0$, $\sigma_{amacrine} = 0.3°$, $a_{ganglion} = 1.0$, $b_{ganglion} = 2.0$, $c_{ganglion} = 0.0$, $\sigma_{ganglion} = 0.1°$, $k_{(f)ganglion} = 0.1$, $\tau_{(s)ganglion} = 10000$ *ms*, $k_{(d)ganglion} = 0.05$.

References

1. S. R. y Cajal, *La rétine des vertébrés* (Typ. de Joseph van In & Cie., 1893).
2. B. B. Lee, P. R. Martin and U. Grünert, Retinal connectivity and primate vision, *Progress in retinal and eye research* **29**(6) (2010) 622–639.
3. T. Gollisch and M. Meister, Eye smarter than scientists believed: neural computations in circuits of the retina, *Neuron* **65**(2) (2010) 150–164.
4. T. Guo, D. Tsai, S. Bai, J. W. Morley, G. J. Suaning, N. H. Lovell and S. Dokos, Understanding the retina: A review of computational models of the retina from the single cell to the network level, *Critical Reviews in Biomedical Engineering* **42**(5) (2014).
5. M. Carandini, J. B. Demb, V. Mante, D. J. Tolhurst, Y. Dan, B. A. Olshausen, J. L. Gallant and N. C. Rust, Do we know what the early visual system does?, *The Journal of Neuroscience* **25**(46) (2005) 10577–10597.
6. M.-O. Gewaltig and M. Diesmann, Nest (neural simulation tool), *Scholarpedia* **2**(4) (2007) p. 1430.
7. M. L. Hines and N. T. Carnevale, The neuron simulation environment, *Neural computation* **9**(6) (1997)

1179–1209.
8. D. F. Goodman and R. Brette, The brian simulator, *Frontiers in neuroscience* **3**(2) (2009) p. 192.
9. J. M. Bower and D. Beeman, *The book of GENESIS: exploring realistic neural models with the GEneral NEural SImulation System* (Springer Science & Business Media, 2012).
10. A. Benoit, A. Caplier, B. Durette and J. Hérault, Using human visual system modeling for bio-inspired low level image processing, *Computer Vision and Image Understanding* **114**(7) (2010) 758–773.
11. A. Wohrer and P. Kornprobst, Virtual retina: a biological retina model and simulator, with contrast gain control, *Journal of computational neuroscience* **26**(2) (2009) 219–249.
12. J. Hérault and B. Durette, Modeling visual perception for image processing, *Computational and Ambient Intelligence*, (Springer, 2007), pp. 662–675.
13. C. A. Morillas, S. F. Romero, A. Martínez, F. J. Pelayo, E. Ros and E. Fernández, A design framework to model retinas, *Biosystems* **87**(2) (2007) 156–163.
14. K. Zaghloul, K. Boahen *et al.*, Optic nerve signals in a neuromorphic chip i: Outer and inner retina models, *Biomedical Engineering, IEEE Transactions on* **51**(4) (2004) 657–666.
15. J. v. van Hateren, L. Rüttiger, H. Sun and B. Lee, Processing of natural temporal stimuli by macaque retinal ganglion cells, *The Journal of neuroscience* **22**(22) (2002) 9945–9960.
16. J. Hérault, A model of colour processing in the retina of vertebrates: From photoreceptors to colour opposition and colour constancy phenomena, *Neurocomputing* **12**(2) (1996) 113–129.
17. R. L. De Valois and K. K. De Valois, A multi-stage color model, *Vision research* **33**(8) (1993) 1053–1065.
18. Z. Li, Different retinal ganglion cells have different functional goals, *International Journal of Neural Systems* **3**(03) (1992) 237–248.
19. Y. Ozuysal and S. A. Baccus, Linking the computational structure of variance adaptation to biophysical mechanisms, *Neuron* **73**(5) (2012) 1002–1015.
20. H. van Hateren, A cellular and molecular model of response kinetics and adaptation in primate cones and horizontal cells, *Journal of vision* **5**(4) (2005) p. 5.
21. C. Enroth-Cugell and J. G. Robson, The contrast sensitivity of retinal ganglion cells of the cat, *The Journal of physiology* **187**(3) (1966) 517–552.
22. B. B. Lee, R. M. Shapley, M. J. Hawken and H. Sun, Spatial distributions of cone inputs to cells of the parvocellular pathway investigated with cone-isolating gratings, *JOSA A* **29**(2) (2012) A223–A232.
23. O. S. Packer and D. M. Dacey, Receptive field structure of h1 horizontal cells in macaque monkey retina, *Journal of Vision* **2**(4) (2002) p. 1.
24. R. A. Young, The gaussian derivative model for spatial vision: I. retinal mechanisms, *Spatial vision* **2**(4) (1987) 273–293.
25. S. Tan, J. L. Dale and A. Johnston, Performance of three recursive algorithms for fast space-variant gaussian filtering, *Real-Time Imaging* **9**(3) (2003) 215–228.
26. B. Triggs and M. Sdika, Boundary conditions for young-van vliet recursive filtering, *Signal Processing, IEEE Transactions on* **54**(6) (2006) 2365–2367.
27. R. Deriche, Fast algorithms for low-level vision, *Pattern Analysis and Machine Intelligence, IEEE Transactions on* **12**(1) (1990) 78–87.
28. R. Deriche, Recursively implementating the gaussian and its derivatives, *Research Report (Inria-00074778)* (1993).
29. M. J. Berry, I. H. Brivanlou, T. A. Jordan and M. Meister, Anticipation of moving stimuli by the retina, *Nature* **398**(6725) (1999) 334–338.
30. V. C. Smith, J. Pokorny, B. B. Lee and D. M. Dacey, Primate horizontal cell dynamics: an analysis of sensitivity regulation in the outer retina, *Journal of Neurophysiology* **85**(2) (2001) 545–558.
31. D. B. Kastner and S. A. Baccus, Coordinated dynamic encoding in the retina using opposing forms of plasticity, *Nature neuroscience* **14**(10) (2011) 1317–1322.
32. A. L. Hodgkin and A. F. Huxley, A quantitative description of membrane current and its application to conduction and excitation in nerve, *The Journal of physiology* **117**(4) (1952) 500–544.
33. A. V. Herz, T. Gollisch, C. K. Machens and D. Jaeger, Modeling single-neuron dynamics and computations: a balance of detail and abstraction, *science* **314**(5796) (2006) 80–85.
34. P. Dayan and L. Abbott, Theoretical neuroscience: computational and mathematical modeling of neural systems, *Journal of Cognitive Neuroscience* **15**(1) (2003) 154–155.
35. B. Hille *et al.*, *Ion channels of excitable membranes* (Sinauer Sunderland, MA, 2001).
36. D. Sterratt, B. Graham, A. Gillies and D. Willshaw, *Principles of computational modelling in neuroscience* (Cambridge University Press, 2011).
37. M. Carandini and D. J. Heeger, Normalization as a canonical neural computation, *Nature Reviews Neuroscience* **13**(1) (2012) 51–62.
38. J. D. Victor, The dynamics of the cat retinal x cell centre., *The Journal of Physiology* **386**(1) (1987) 219–246.
39. V. Mante, V. Bonin and M. Carandini, Functional mechanisms shaping lateral geniculate responses to artificial and natural stimuli, *Neuron* **58**(4) (2008) 625–638.
40. M. Carandini, D. J. Heeger and J. A. Movshon, Linearity and normalization in simple cells of the macaque primary visual cortex, *The Journal of Neuroscience* **17**(21) (1997) 8621–8644.
41. K. Purpura, D. Tranchina, E. Kaplan and R. M.

Shapley, Light adaptation in the primate retina: analysis of changes in gain and dynamics of monkey retinal ganglion cells, *Visual neuroscience* **4**(01) (1990) 75–93.
42. V. Torre and T. Poggio, A synaptic mechanism possibly underlying directional selectivity to motion, *Proceedings of the Royal Society of London. Series B. Biological Sciences* **202**(1148) (1978) 409–416.
43. F. R. Amthor and N. M. Grzywacz, Nonlinearity of the inhibition underlying retinal directional selectivity, *Visual neuroscience* **6**(03) (1991) 197–206.
44. R. R. Harrison and C. KocH, An analog vlsi inplementation of a visual interneuron: Enhanced sensory processing through biophysical modeling, *International Journal of Neural Systems* **9**(05) (1999) 391–395.
45. R. A. Silver, Neuronal arithmetic, *Nature Reviews Neuroscience* **11**(7) (2010) 474–489.
46. S. A. Baccus and M. Meister, Fast and slow contrast adaptation in retinal circuitry, *Neuron* **36**(5) (2002) 909–919.
47. F. Rieke, Temporal contrast adaptation in salamander bipolar cells, *The Journal of Neuroscience* **21**(23) (2001) 9445–9454.
48. K. J. Kim and F. Rieke, Temporal contrast adaptation in the input and output signals of salamander retinal ganglion cells, *The Journal of Neuroscience* **21**(1) (2001) 287–299.
49. D. Chander and E. Chichilnisky, Adaptation to temporal contrast in primate and salamander retina, *The Journal of Neuroscience* **21**(24) (2001) 9904–9916.
50. K. A. Zaghloul, K. Boahen and J. B. Demb, Different circuits for on and off retinal ganglion cells cause different contrast sensitivities, *The Journal of Neuroscience* **23**(7) (2003) 2645–2654.
51. R. S. Zucker and W. G. Regehr, Short-term synaptic plasticity, *Annual review of physiology* **64**(1) (2002) 355–405.
52. M. Tsodyks and S. Wu, Short-term synaptic plasticity, *Scholarpedia* **8**(10) (2013) p. 3153.
53. B. Suh and S. A. Baccus, Building blocks of temporal filters in retinal synapses, *PLoS Biol* **12**(10) (2014) p. e1001973.
54. D. L. Beaudoin, M. B. Manookin and J. B. Demb, Distinct expressions of contrast gain control in parallel synaptic pathways converging on a retinal ganglion cell, *The Journal of physiology* **586**(22) (2008) 5487–5502.
55. M. B. Manookin and J. B. Demb, Presynaptic mechanism for slow contrast adaptation in mammalian retinal ganglion cells, *Neuron* **50**(3) (2006) 453–464.
56. B. P. Ölveczky, S. A. Baccus and M. Meister, Retinal adaptation to object motion, *Neuron* **56**(4) (2007) 689–700.
57. J. B. Demb, Functional circuitry of visual adaptation in the retina, *The Journal of physiology* **586**(18) (2008) 4377–4384.
58. F. S. Chance, S. B. Nelson and L. F. Abbott, Synaptic depression and the temporal response characteristics of v1 cells, *The Journal of neuroscience* **18**(12) (1998) 4785–4799.
59. M. Carandini, D. J. Heeger and W. Senn, A synaptic explanation of suppression in visual cortex, *The Journal of Neuroscience* **22**(22) (2002) 10053–10065.
60. D. Tschumperlé, The cimg library, *IPOL 2012 Meeting on Image Processing Libraries*, 2012, pp. 4–pp.
61. O. Estévez, On the fundamental data-base of normal and dichromatic colour vision, PhD thesis, University of Amsterdam (1979).
62. S. Ghosh-Dastidar and H. Adeli, Spiking neural networks, *International Journal of Neural Systems* **19**(04) (2009) 295–308.
63. B. B. Lee, D. M. Dacey, V. C. Smith and J. Pokorny, Dynamics of sensitivity regulation in primate outer retina: The horizontal cell network, *Journal of Vision* **3**(7) (2003) p. 5.
64. F. A. Dunn, M. J. Lankheet and F. Rieke, Light adaptation in cone vision involves switching between receptor and post-receptor sites, *Nature* **449**(7162) (2007) 603–606.
65. D. Tranchina, J. Gordon and R. Shapley, Retinal light adaptation-evidence for a feedback mechanism, *Nature* **310**(5975) (1984) 314–316.
66. V. C. Smith, J. Pokorny, B. B. Lee and D. M. Dacey, Sequential processing in vision: The interaction of sensitivity regulation and temporal dynamics, *Vision research* **48**(26) (2008) 2649–2656.
67. D. A. Clark, R. Benichou, M. Meister and R. A. da Silveira, Dynamical adaptation in photoreceptors (2013).
68. J. B. Demb, Multiple mechanisms for contrast adaptation in the retina, *Neuron* **36**(5) (2002) 781–783.
69. D. L. Beaudoin, B. G. Borghuis and J. B. Demb, Cellular basis for contrast gain control over the receptive field center of mammalian retinal ganglion cells, *The Journal of neuroscience* **27**(10) (2007) 2636–2645.
70. K. J. Kim and F. Rieke, Slow na+ inactivation and variance adaptation in salamander retinal ganglion cells, *The Journal of neuroscience* **23**(4) (2003) 1506–1516.
71. P. Martínez-Cañada, C. Morillas, S. Romero and F. Pelayo, Modeling retina adaptation with multiobjective parameter fitting, *Advances in Computational Intelligence*, (Springer, 2015), pp. 175–184.
72. P. Martínez-Cañada, C. Morillas, B. Pino and F. Pelayo, Towards a generic simulation tool of retina models, *Artificial Computation in Biology and Medicine*, (Springer, 2015), pp. 47–57.
73. K. A. Zaghloul, K. Boahen and J. B. Demb, Contrast adaptation in subthreshold and spiking responses of mammalian y-type retinal ganglion cells, *The Journal of neuroscience* **25**(4) (2005) 860–868.
74. B. P. Ölveczky, S. A. Baccus and M. Meister, Segregation of object and background motion in the retina, *Nature* **423**(6938) (2003) 401–408.
75. S. A. Baccus, B. P. Ölveczky, M. Manu and M. Meis-

ter, A retinal circuit that computes object motion, *The Journal of Neuroscience* **28**(27) (2008) 6807–6817.

76. J. B. Demb, K. Zaghloul, L. Haarsma and P. Sterling, Bipolar cells contribute to nonlinear spatial summation in the brisk-transient (y) ganglion cell in mammalian retina, *The Journal of neuroscience* **21**(19) (2001) 7447–7454.
77. P. Martínez-Cañada, C. Morillas, J. L. Nieves, B. Pino and F. Pelayo, First stage of a human visual system simulator: The retina, *Computational Color Imaging*, (Springer, 2015), pp. 118–127.
78. J. D. Crook, C. M. Davenport, B. B. Peterson, O. S. Packer, P. B. Detwiler and D. M. Dacey, Parallel on and off cone bipolar inputs establish spatially coextensive receptive field structure of blue-yellow ganglion cells in primate retina, *The Journal of Neuroscience* **29**(26) (2009) 8372–8387.
79. N. Srinivas and K. Deb, Muiltiobjective optimization using nondominated sorting in genetic algorithms, *Evolutionary computation* **2**(3) (1994) 221–248.
80. W. Van Geit, E. De Schutter and P. Achard, Automated neuron model optimization techniques: a review, *Biological cybernetics* **99**(4-5) (2008) 241–251.
81. J. C. da Silva Martins, Computational models, neuronal metrics and system identification in bioelectronic vision, PhD thesis (2012).
82. S. Druckmann, Y. Banitt, A. Gidon, F. Schürmann, H. Markram and I. Segev, A novel multiple objective optimization framework for constraining conductance-based neuron models by experimental data, *Frontiers in neuroscience* **1**(1) (2007) p. 7.